Available online at www.sciencedirect.com
ScienceDirect
Journal of Physics and Chemistry of Solids 67 (2006) 2001–2006
JOURNAL OF PHYSICS AND CHEMISTRY OF SOLIDS
www.elsevier.com/locate/jpcs

Effect of high-current pulsed electron beam irradiation on the structure of $La_{0.7}Sr_{0.3}CoO_3$ powder

V.V. Efimov[a,*], E.A. Efimova[a], K. Iakoubovskii[b], D.V. Karpinskii[c], S. Khasanov[d], D.I. Kochubey[e], V.V. Kriventsov[e], A. Kuzmin[f], A.P. Sazonov[c], V. Sikolenko[g], M. Sakharov[d], A.N. Shmakov[e], S.I. Tiutiunnikov[a]

[a]*Joint Institute for Nuclear Research, 141980 Dubna, Moscow region, Russia*
[b]*Katholieke Universiteit Leuven, Celestijnenlaan 200 D, 3001 Leuven, Belgium*
[c]*Institute of Solid State and Semiconductor Physics, 220072 Minsk, Belarus*
[d]*Institute of Solid State Physics, RAS Chernogolovka, Moscow region, Russia*
[e]*Boreskov Institute of Catalysis, Lavrentiev prosp. 5, Novosibirsk 630090, Russia*
[f]*Institute of Solid State Physics, Kengaraga str. 8, LV-1063 Riga, Latvia*
[g]*Hahn-Meitner-Institut Glienicker str. 100, Berlin D-14109, Germany*

Abstract

The effect of pulsed electron irradiation on the long- and short-range order in the $La_{0.7}Sr_{0.3}CoO_3$ ceramics is reported. Neutron and X-ray powder diffraction reveal that the unit cell symmetry and single-phase state of single and multiple irradiated $La_{0.7}Sr_{0.3}CoO_3$ are preserved, while the oxygen atoms coordination changes towards the $La_{0.5}Sr_{0.5}CoO_3$ structure. X-ray absorption data confirm this observation and further reveal the details of the shift and splitting of the Co^{3+} t_{2g} and e_g atomic orbitals. Possible mechanisms of pulsed electron irradiation effect in $La_{0.7}Sr_{0.3}CoO_3$ are discussed.

PACS: 61.10.Nz; 61.10.Ht; 61.12.Ld; 61.80.X

Keywords: A. Ceramics; C. XAFS (EXAFS and XANES); C. X-ray diffraction; D. Defects; D. Radiation damage

1. Introduction

The discovery of the "colossal" magnetoresistance (CMR) in the manganites with perovskite structure [1] has stimulated search for the compounds exhibiting large magnetoresistance. Large magnetoresistance was obtained in $La_{1-x}Sr_xCoO_3$ with $0.15 \leqslant x \leqslant 0.2$ [2]. However, ferromagnetic ordering in $La_{1-x}Sr_xCoO_3$ does not lead to a metal–insulator transition like in CMR materials [3,4]. In addition, $La_{1-x}Sr_xCoO_3$ compounds are technologically important because of their catalytic properties and possibilities to use them as electrode material in solid-oxide fuel cells and as a membrane in oxygen separation processes [5].

The magnetic and transport properties of $La_{1-x}Sr_xCoO_3$ cobaltites with perovskite structure and of manganites, such as $La_{1-x}Sr_xMnO_3$, exhibit common features [6]: In both systems the substitution of La^{3+} with Sr^{2+} ion creates paramagnetic ($x<0.15$) to ferromagnetic ($x>0.3$) transition as the dopant concentration is increased. In addition to their large thermomagnetic irreversibility, these compounds also show interesting changes in their magnetic and transport properties as the average size of the ions at the rare-earth site varies. The unusual properties of the cobaltites are also reflected in the observation of giant anisotropic magnetostriction [7], which has been explained on the basis of a spin state transition from the low-spin (LS, $t_{2g}^6 e^0{}_g$) Co^{3+} configuration with spherical electron

*Corresponding author. Tel.: +7 09621 64173; fax: +7 09621 65767.
E-mail addresses: klevcova@sunse.jinr.ru, vadim.efimov@sunse.jinr.ru (V.V. Efimov).

0022-3697/$ - see front matter © 2006 Elsevier Ltd. All rights reserved.
doi:10.1016/j.jpcs.2006.05.033

cloud and zero orbital momentum to the Jahn–Teller distorted intermediate-spin (IS) (IS, $t_{2g}^5 e^1{}_g$) Co^{4+} configuration with a finite orbital momentum. Most studies on the spin states of Co ions suggest that the trivalent and tetravalent cobalt ions remain as a mixture of LS and IS states [8].

It is well known that all those remarkable properties of $La_{1-x}Sr_xCoO_3$ ceramics crucially depend on their lattice structure and are particularly affected by structural distortions around the transition-metal sites [9]. Therefore, in order to characterize such lattice distortions, in the present work, we precisely determined, using high-resolution powder X-ray and neutron diffraction techniques, the lattice parameter, interatomic distances and especially displacements of oxygen ions in $La_{0.7}Sr_{0.3}CoO_3$ ceramics irradiated by high-current pulsed electron beam. In addition, the local atomic and electronic structure at the Co *K*-edge in these samples is characterized by extended X-ray absorption spectroscopy. The sensitivity of extended X-ray absorption fine structure (EXAFS) and X-ray absorption near edge structure (XANES) to chemical composition, local lattice distortion and to an overlapping mixture of IS $^3T_1$ ($t_{2g}^5 e_g^1$) and high-spin (HS) $^5T_2$ ($t_{2g}^4 e_g^2$) states of Co^{3+} in these cobaltites is revealed. The correlation of the crystallographic parameter changes in $La_{1-x}Sr_xCoO_3$ ($x = 0.3$ and 0.5) and irradiated $La_{0.7}Sr_{0.3}CoO_3$ samples and local atomic and electronic structure around cobalt ions is also discussed.

2. Experimental procedures

Solutions of lanthanum nitrate ware prepared by dissolving lanthanum oxide in nitric acid. They were characterized by EDTA titration and mixed together with the cation ratio corresponding to the stoichiometry of the $La_{1-x}Sr_xCoO_3$ ($x = 0.3$ and 0.5). Solutions were frozen by spraying through a pneumatic nozzle into liquid nitrogen. After evaporation of nitrogen the metal trays with the frozen granules were transferred to the shelves of an SMH-15 freeze-drier (Usifroid) precooled to 200 K. Freeze-drying was carried out at $p = 4 \times 10^2$ mbar for 48 h while the temperature of the heating shelves was raised from −50 to +50 °C. The obtained powder was decomposed in air at 250 °C. The product was re-grinned, pressed into pellets and then optically polished to 1 mm thickness, in order to maximize the electron irradiation effects (see a comment below). They were further annealed in air at 500 °C and then at 1000 °C for 24 h. The samples were stoichiometric, with no impurities detectable by the X-ray analysis.

The samples were irradiated by pulsed electron beam from the linear inductive accelerator LIU 3000 [10] using the following parameters: energy 800 keV, beam current 200 A, pulse duration 2×10^{-7} s, repetition rate 0.5 Hz, beam diameter 20 mm, and doses 6×10^{14} (1 pulse = 1 k) and 6×10^{15} (10 pulses = 10 k) electrons/cm^2 at nominally room temperature. The penetration depth of 800 keV electrons into $La_{1-x}Sr_xCoO_3$ ceramics is ~0.9 mm [11]. Note, that the electron irradiation effects in $La_{1-x}Sr_xCoO_3$ ceramics are maximal when this penetration depth is similar to the sample thickness [12].

X-ray experimental data were collected with a Siemens D500 diffractometer (Bragg–Brentano geometry) using Cu$K_{\alpha 1}$ radiation with $\lambda = 1.5406$ Å at 30 kV, 30 mA and SiO_2-monochromator, Ni-filter and a position-sensitive detector in steps of 0.02° at room temperature. Some X-ray diffraction peaks were measured at Siberian Synchrotron Radiation Center using high-resolution powder diffractometer at room temperature. Monochromatization of primary Synchrotron Radiation beam was performed by Si(1 1 1) monochromator. Radiation wavelength was 1.5398 Å. Diffractometer is equipped by Ge(1 1 1) crystal analyzer on the diffracted beam providing extremely high instrumental resolution and accuracy of data. For X-ray diffraction measurements the irradiated ceramic samples were grinded into powder. The data were analyzed using the Powder Cell program [13].

The neutron powder diffraction experiments were carried out on the fine resolution neutron diffractometer E9 at the BER-II reactor in Hahn Meitner Institute [14]. Data were collected at 290 K over the range $4 \leqslant 2\theta \leqslant 156°$ with the wavelength $\lambda = 1.7973$ Å.

The Co *K*-edge ($E_K = 7710$ eV) EXAFS spectra were recorded at the EXAFS station of Siberian Synchrotron Radiation Center. The storage ring VEPP-3 with electron beam energy of 2 GeV and an average stored current of 80 mA was used as the radiation source. The X-ray energy was monochromatized with a channel-cut Si(1 1 1) crystal monochromator. The Co *K*-edge EXAFS spectra were recorded in transmission mode, using two ionization chambers, filled with argon gas, as detectors. The energy step was ~2.5 eV. The samples were prepared as pellets with the varied thickness to obtain a 0.7–1.0 absorption edge jump.

The EXAFS spectra were processed using the standard VIPER package [15]. The energy position E_0, used in the definition of the photoelectron wave number $k = [2(E - E_0)me/\hbar^2]^{0.5}$, was set at the threshold energy of 7710 eV. The Fourier transforms (FTs) of the EXAFS $k^3\chi(k)$ spectra were calculated in the wave number interval $k = 2.0$–12 Å^{-1} with a Gaussian-type window function. A curve fitting procedure with the IFEFFIT 1.2.6 [16] code was used to determine precisely the distances, Debye–Waller factors and coordination numbers for the first two coordination shells in similar wave number intervals. The input file for FEFF6 was constructed using the ATOMS code based on a set of refined neutron diffraction data for the $La_{0.7}Sr_{0.3}CoO_3$ before and after irradiation (see below).

The XANES data analysis in the range 7690–7730 eV was performed with the program WINXAS [17]. The data were normalized by setting a point located at about 200 eV above the edge to unity.

3. Results and analysis

3.1. X-ray diffraction results

Fig. 1 shows experimental and calculated XRD profiles for the unirradiated $La_{0.7}Sr_{0.3}CoO_3$ powder. The obtained structural data are given in Table 1. They are in agreement with previous studies [18,19].

Table 1 and inset in Fig. 1 reveal that single and multiple irradiation of the $La_{0.7}Sr_{0.3}CoO_3$ do not lead to the essential changes in the lattice parameters and unit cell symmetry, whereas an intensity redistribution upon irradiation is observed for the $(1\,\bar{1}\,0)$ and $(2\,1\,1)$ reflections. The Rietveld profile refinment suggests that this intensity redistribution upon irradiation is related to the shift of oxygen atoms. A similar shift is observed upon Sr doping (see Table 1).

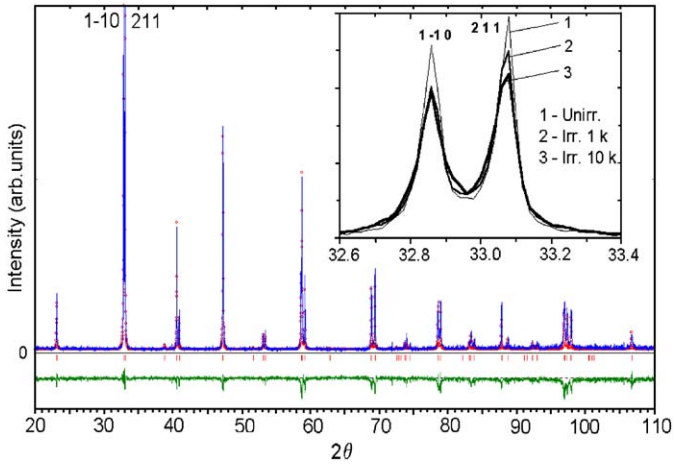

Fig. 1. Room-temperature Rietveld refinement plot of X-ray diffraction pattern for unirradiated $La_{0.7}Sr_{0.3}CoO_3$ ceramics. The observed and calculated patterns are shown by solid line and dots, respectively. The vertical marks show the positions of calculated reflections. The bottom trace is the difference between the observed and calculated spectra. The inset highlights the behavior of the $(1\,\bar{1}\,0)$ and $(2\,\bar{1}\,1)$ reflections for unirradiated and irradiated by one (1 k) and ten electron pulses (10 k) samples.

3.2. Neutron diffraction results

The room-temperature data for unirradiated $La_{0.5}Sr_{0.5}CoO_3$ and for unirradiated and irradiated $La_{0.7}Sr_{0.3}CoO_3$ ceramics were analyzed by the profile refinement method. The result of Rietveld refinement for the $La_{0.7}Sr_{0.3}CoO_3$ is presented in Fig. 2.

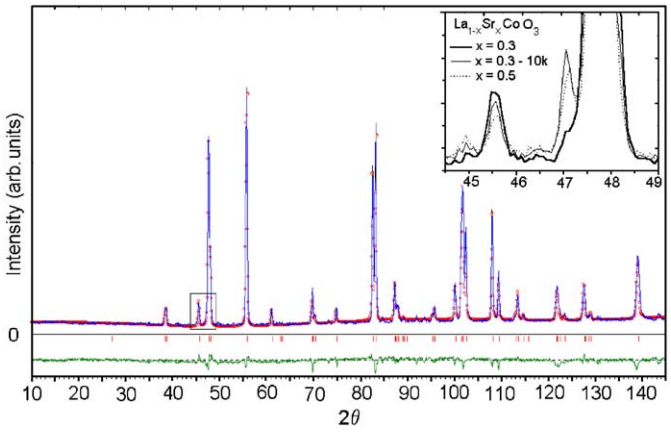

Fig. 2. Neutron diffraction pattern of unirradiated $La_{0.7}Sr_{0.3}CoO_3$ at room temperature: experimental curve (continuous line), refinement points (open circles) and their difference (continuous line below). Ticks show the predicted 2θ positions for the Bragg peaks. The inset shows the structure of the $(1\,\bar{1}\,1)$ peak in unirradiated $La_{0.7}Sr_{0.3}CoO_3$ and $La_{0.5}Sr_{0.5}CoO_3$ samples, and ten-pulse (10 k) electron-irradiated $La_{0.7}Sr_{0.3}CoO_3$ ceramics.

Table 1
Structural parameters for unirradiated $La_{1-x}Sr_xCoO_3$ ($x = 0.3$ and 0.5) ceramics and for single-pulse (1 k) and ten-pulse (10 k) electron-irradiated $La_{0.7}Sr_{0.3}CoO_3$ sample, obtained by X-ray diffraction

Sample		$x = 0.3$	$x = 0.3$, 1 k irr.	$x = 0.3$, 10 k irr.	$x = 0.5$
Space group		$R\bar{3}C$	$R\bar{3}C$	$R\bar{3}C$	$R\bar{3}C$
a (Å)		5.4081 (2)	5.4082 (3)	5.4090 (3)	5.4131 (2)
b (Å)		5.4081 (2)	5.4082 (3)	5.4090 (3)	5.4131 (2)
c (Å)		5.4081 (3)	5.4082 (3)	5.4090 (3)	5.4131 (2)
α (deg)		60.412 (2)	60.411 (2)	60.407 (2)	60.152 (2)
V (Å^3)		113.067	113.069	113.197	113.320
La/Sr	x	0.250	0.250	0.250	0.250
	y	0.250	0.250	0.250	0.250
	z	0.250	0.250	0.250	0.250
Co	x	0.000	0.000	0.000	0.000
	y	0.000	0.000	0.000	0.000
	z	0.000	0.000	0.000	0.000
O	x	0.208 (3)	0.215 (3)	0.222 (3)	0.243 (3)
	y	0.290 (3)	0.283 (3)	0.273 (3)	0.259 (3)
	z	0.750	0.750	0.750	0.750
R_{wp}(%)		16.21	17.46	17.83	14.35

R_{wp} is a reliability factor.

Some structural parameters calculated from the neutron diffraction patterns are presented in Table 2. It should be noted that multiple irradiation of $La_{0.7}Sr_{0.3}CoO_3$ decreases the $(1\bar{1}1)$ peak intensity that corresponds to the decrease of the oxygen octahedra asymmetry [20]. Similar to the XRD results of Table 1, the result of Rietveld refinement for the irradiated $La_{0.7}Sr_{0.3}CoO_3$ ceramics reveals the changes of the oxygen atoms positions similar to those observed upon Sr doping. Moreover, a similar structure appears around the $(1\bar{1}1)$ peak either upon irradiation or Sr doping (see inset in Fig. 2).

3.3. X-ray absorption results

3.3.1. EXAFS spectra

The FTs of the Co *K*-edge EXAFS spectra (see Fig. 3) for the unirradiated $La_{1-x}Sr_xCoO_3$ ($x = 0.3$ and 0.5) and ten-pulse (10 k) irradiated $La_{0.7}Sr_{0.3}CoO_3$ samples are presented in Fig. 4.

The first strong peak is due to the contribution from the first coordination shell, formed by six oxygen atoms and located at 1.93 Å. The group of peaks in the range 2.2–4.3 Å is attributed to four contributions: (1) the multiple-scattering signals generated within the first shell, which we neglect in the present analysis; (2) eight La/Sr atoms located in the second shell; (3) six Co atoms in the third shell and multiple-scattering signals generated in Co–O–Co chains; (4) 24 oxygen atoms in the fourth shell. Preliminary quantitative analysis was performed for the first two peaks appearing in the FTs from all samples between $R = 1.0$ and 4.5 Å (Fig. 4) by fitting them to simplified model, containing a set of theoretical scattering pathways pertinent to the space group $R\bar{3}C$ lattice symmetry (Table 3).

Substitution of La^{3+} for Sr^{2+} in $La_{1-x}Sr_xCoO_3$ does not modify significantly the interatomic distances within the first three coordination shells (Table 3). Only weak increase of the Co–Co interatomic distances of about 0.02 Å is observed for the third coordination shell. Note that some change in the shape of the second peak, observed in the FT of the EXAFS signals in Fig. 3, is related mainly to the difference in the scattering amplitudes of La and Sr ions. It should be noted, that no essential structural changes were observed for the $La_{0.7}Sr_{0.3}CoO_3$ sample after multiple electron irradiation (Table 3).

3.3.2. XANES spectra

The dipole-allowed $1s \rightarrow np$ transitions at the Co *K*-edge dominate the XANES spectrum shown in Fig. 5. The *d*

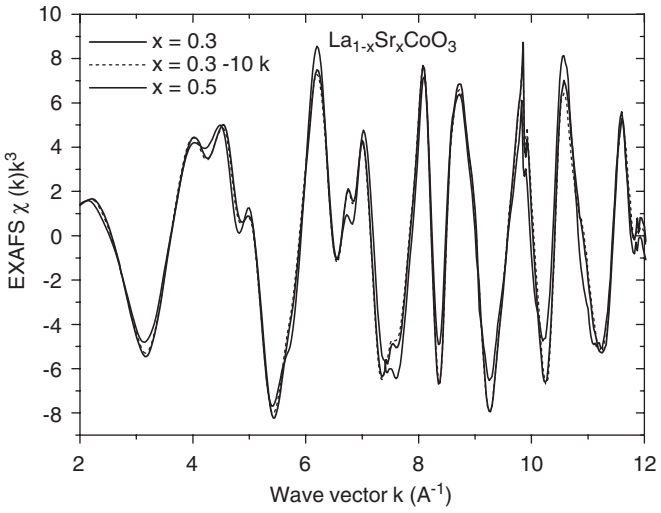

Fig. 3. Experimental EXAFS $\chi(k)k^3$ signals at the Co *K*-edge in unirradiated $La_{0.7}Sr_{0.3}CoO_3$ and $La_{0.5}Sr_{0.5}CoO_3$ and multiple (10 k) irradiated $La_{0.7}Sr_{0.3}CoO_3$ powders.

Table 2
Structural parameters for unirradiated $La_{1-x}Sr_xCoO_3$ ($x = 0.3$ and 0.5) ceramics and for ten-pulse (10 k) electron-irradiated $La_{0.7}Sr_{0.3}CoO_3$ sample, obtained by neutron diffraction

Sample		$x = 0.3$	$x = 0.3$, 10 k irr.	$x = 0.5$
Space group		$R\bar{3}C$	$R\bar{3}C$	$R\bar{3}C$
a (Å)		5.411 (2)	5.413 (2)	5.417 (2)
b (Å)		5.411 (2)	5.413 (2)	5.417 (2)
c (Å)		5.411 (2)	5.413 (2)	5.417 (2)
α (deg)		60.416 (2)	60.404 (2)	60.147 (2)
V (Å^3)		113.079	113.175	113.288
	x	0.250	0.250	0.250
La/Sr	y	0.250	0.250	0.250
	z	0.250	0.250	0.250
	x	0.000	0.000	0.000
Co	y	0.000	0.000	0.000
	z	0.000	0.000	0.000
O	x	0.211 (4)	0.229 (4)	0.251 (4)
	y	0.296 (4)	0.275 (4)	0.256 (4)
	z	0.750(4)	0.750(4)	0.750(4)
R_{wp}(%)		18.34	19.93	17.21

R_{WP} is a reliability factor.

orbitals of cobalt mix heavily with the oxygen $2p$ orbitals [21] and the cobalt t_{2g} and e_g orbitals are expected to split by the crystal field and by the interatomic exchange energy (Hund's rule coupling) [22]. Although the $1s \rightarrow t_{2g}$ and $1s \rightarrow e_g$ transitions are forbidden in the dipole approximation, they could be experimentally observed because of oxygen p state admixing and quadrupole transitions [23]. Therefore, we attribute the pre-edge peak, appearing in Fig. 5 below 7715 eV, to the $1s \rightarrow 3d$ transition, which energy position can be used to evaluate the valence state of cobalt. The intra-atomic exchange energy could result in additional unresolved splitting of the t_{2g} and e_g bands, thus contributing to the observed peak broadening (Fig. 5). Note that this interatomic exchange splitting could actually be comparable with the crystal field splitting [24]. An additional minor splitting is also expected from the Jahn–Teller distortions.

Substitution of La^{3+} for Sr^{2+} in $La_{1-x}Sr_xCoO_3$ ceramics leads to the small but observable edge shift of about 0.5 eV for both the t_{2g} and e_g bands to the lower energies (see the inset of Fig. 5). It should be noted, that no essential changes of the t_{2g} and e_g bands position was observed for the $La_{0.7}Sr_{0.3}CoO_3$ sample after multiple irradiation (see Fig. 5).

4. Conclusions

XRD and neutron diffraction results (Figs. 1, 2 and Tables 1, 2) reveal changes in the long-range order of $La_{0.7}Sr_{0.3}CoO_3$ induced by ten-pulse electron irradiation. However, EXAFS and XANES spectra do not detect significant local atomic and electron structure transformations. This effect could possibly be attributed to (i) selective nature of our X-ray absorption experiments (only local

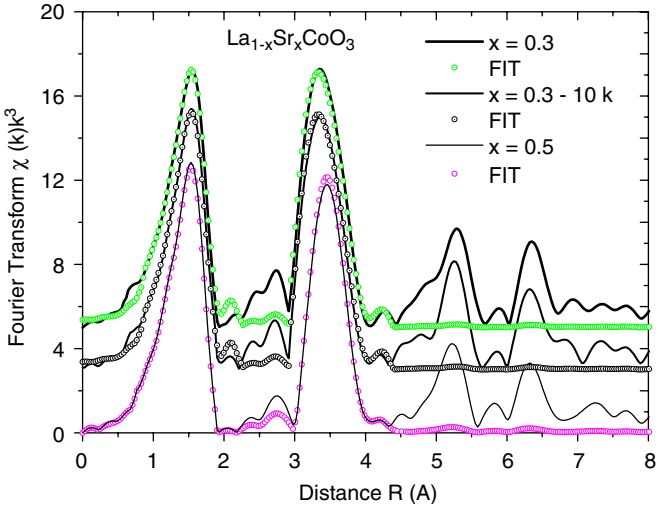

Fig. 4. Experimental (—) and fitted (o) Fourier transforms of the Co K-edge EXAFS $\chi(k)k^3$ signals for the unirradiated $La_{0.7}Sr_{0.3}CoO_3$ and $La_{0.5}Sr_{0.5}CoO_3$ powders and ten-pulse (10 k) electron-irradiated $La_{0.7}Sr_{0.3}CoO_3$ sample.

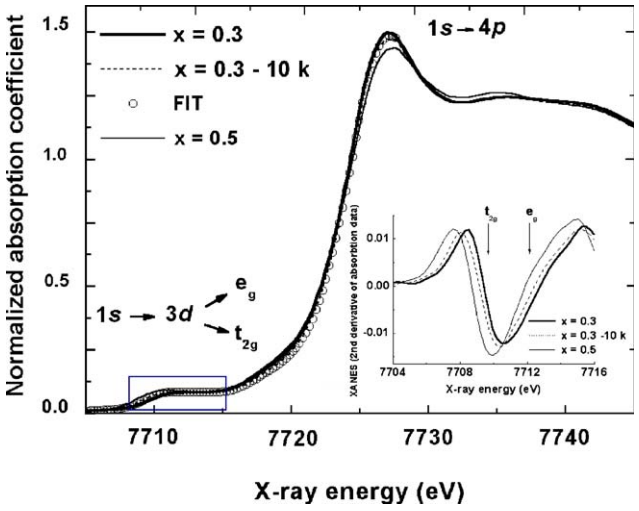

Fig. 5. Experimental (—) and calculated (o) Co K-edge XANES spectra for $La_{1-x}Sr_xCoO_3$ ($x = 0.3$ and 0.5) and multiple (10 k) irradiated $La_{0.7}Sr_{0.3}CoO_3$.

Table 3
Structural parameters derived from the Co K-edge EXAFS analysis (see Fig. 4) for unirradiated $La_{1-x}Sr_xCoO_3$ ($x = 0.3$ and 0.5) ceramics and ten-pulse (10 k) electron-irradiated $La_{0.7}Sr_{0.3}CoO_3$ sample: scattering path, coordination number (CN), interatomic distance (R, Å), residuals (i.e., deviation between experimental data and fit, %) and Debye–Waller factors (σ^2, $Å^2 \times 10^{-3}$)

Path	$x = 0.3$			$x = 0.3$, 10 k irr.			$x = 0.5$	
	CN	R	σ^2	R	σ^2	CN	R	σ^2
Co–O	6	1.93 (1)	4.5	1.93 (1)	4.7	6	1.94 (1)	4.4
Co–La	2.8	3.28 (1)	12.4	3.28 (1)	12.5	2	3.29 (1)	12.1
Co–Sr	1.2	3.28 (1)	12.7	3.28 (1)	12.9	2	3.29 (1)	12.6
Co–La	2.8	3.33 (1)	5.6	3.33 (1)	5.7	2	3.34 (1)	5.5
Co–Sr	1.2	3.33 (1)	5.8	3.33 (1)	5.9	2	3.34 (1)	5.8
Co–Co	6	3.83 (1)	10.1	3.83 (1)	10.3	6	3.85 (1)	9.9
Co–O–Co	12	3.85 (1)	9.3	3.85 (1)	9.5	12	3.89 (1)	9.1
Co–O–Co–O	6	3.87 (1)	9.7	3.88 (1)	9.9	6	3.93 (1)	9.6
Residual (%)	—	2.31	—	2.64	—	—	2.23	—

The data were generated with the FEFF6 code [16] and the structural data for space groups $R\bar{3}C$.

coordination of Co atoms has been probed), (ii) lower spectral resolution of X-ray absorption as compared to diffraction techniques.

Regarding the multiple-pulse irradiation, it is important to note that both the pulse duration (2×10^{-7} s) and electron–ion relaxation processes ($\sim10^{-12}$ s) in $La_{0.7}Sr_{0.3}CoO_3$ are much faster than the acoustic discharge processes ($\sim4\times10^{-5}$ s). Therefore, this material can not release energy, accumulated under pulsed electron irradiation, by usual thermal expansion. Instead, due to the asymmetric shape of the vibrational potential, compression or so-called thermal shock phenomenon is observed [12]. Moreover, it has been noted that multiple irradiation can result in heating of $La_{0.7}Sr_{0.3}CoO_3$ sample up to $\sim500\,^{\circ}C$ accompanied by significant increase in diffusion of vacancies and interstitials. The latter could lead to the recrystallization and corresponding increase of lattice volume and in the ion oxygen shift towards $La_{0.5}Sr_{0.5}CoO_3$ structure (see Table 1, 2), as compared to unirradiated material.

Acknowledgments

V.E. and E.E. are grateful to Vice-director JINR Professor A.N. Sissakian and Russian Basic Research Foundation for financial support for participating in the SMEC-2005. V.E. thanks Professor V.L. Aksenov for support during the XRD, Neutron diffraction, EXAFS and Raman experiments. We also thank Dr. A.A. Kaminsky and his group for providing irradiation opportunity at LIU-3000 and for technical assistance.

References

[1] P.M. Raccah, J.B. Goodenough, Phys. Rev. 155 (1967) 932.
[2] G. Briceno, et al., Science 270 (1995) 273.
[3] I. Troyanchuk, et al., J. Phys.: Condens. Mater. 12 (2000) 2485.
[4] R. Caciuffo, et al., Phys. Rev. B 59 (1999) 1068.
[5] R. Sonntag, et al., Physica B 393 (1998) 241–243.
[6] M. Itoh, et al., J. Phys. Soc. Japan 63 (1994) 1486.
[7] M.R. Ibarra, R. Mahandiram, et al., Phys. Rev. B 57 (1998) R3217.
[8] D. Louca, J.L. Sarrao, J.D. Thompson, H. Roder, Phys. Rev. 60 (1999) 10378.
[9] P. Ravindran, P. Blaha, et al., J. Appl. Phys. 91 (2002) 291.
[10] A.A. Kaminsky, V.P. Sarantsev, A.P. Sergeev, Part. Accel. 33 (1990) 189.
[11] V.V. Efimov, S.S. Khasanov, B.N. Mavrin, et al., Ferroelectrics 285 (2003) 265.
[12] V.I. Boiko, A.N. Valyev, A.D. Pogrebnyk, Sov. Phys. Uspekhi 42 (1999) 11.
[13] W. Kraus, G. Nolze, J. Appl. Crystallogr. 29 (1996) 301.
[14] D. Tobbens, N. Stuber, K. Knorr, et al., Mater. Sci. Forum 288 (2001) 378–381.
[15] K.V. Klementev, J. Phys. D: Appl. Phys. 34 (2001) 209–217.
[16] J. Rehr, S. Zabinsky, R. Albers, J. Am. Chem. Soc. 113 (1991) 5135.
[17] T. Ressler, J. Synchrotron Radiat. 5 (1998) 118.
[18] A. Filipponi, J. Phys. B 33 (2000) 2835.
[19] A. Mineshige, M. Inaba, et al., J. Solid State Chem. 121 (1996) 423.
[20] V. Sathe, A. Pimpale, et al., J. Phys.: Condens. Mater. 8 (1996) 3889.
[21] D. Koningsberger, R. Prins, X-ray Absorption, Principles, Applications, Techniques of EXAFS, SEXAFS and XANES, Wiley, New York, 1988 (p. 11).
[22] C. Zobel, M. Kriener, et al., Phys. Rev. B 66 (2002) 020402.
[23] A. Bianconi, et al., Phys. Rev. B 26 (1982) 2741.
[24] O. Toulemonde, N. N'Guyen, F. Studer, J. Solid State Chem. 158 (2001) 208.